Structural Considerations in the Development of an Extremely Lightweight Decelerator

PETER G. NIEDERER*
Astro Research Corporation, Santa Barbara, Calif.

Current development of the Stokes-flow decelerator is aimed at increasing the altitude and improving the quality of atmospheric data sampling of rocket-borne radiosondes. This very lightweight decelerator is expected to support instrumentation weighing 0.175 kg, and to descend with subsonic velocity from altitudes of 80–90 km. Its two distinctive features are: 1) its large flat open mesh filament canopy of low-surface density and high-viscous drag efficiency, and 2) its need for structural support members in the canopy. Several parachute configurations are described; aspects of their structural designs are presented, and their influence on descent performance is outlined. Characteristics of parachutes for small payload weights are analyzed, and configurations are compared using criteria of weight, packability, and deployability combined. Results of theoretical structural analyses of braces are checked by experiments with subscale model parachutes.

Nomenclature

A = projected area of inflated parachute
A' = canopy surface area
B = structural brace parameter
C_D = $2D/v_0^2\rho_a$ drag coefficient of parachute
D = drag force
E = modulus of elasticity
F_0, F_1 = vertical components of forces at canopy attachment points (see Fig. 7)
H_1 = tension force per unit width of load carrying canopy tape (see Fig. 7)
J = moment of inertia
K = canopy loading factor, Eq. (8)
L = brace loading factor, Eq. (11)
M = moment
R = characteristic radius of quasibiconvex foldable column
T_0, T_1 = tension forces in diagonal canopy tension tapes
W = weight
a = A'/A
b = m/AC_D ballistic coefficient
c = empirical constant, Eq. (14)
$f(x)$ = distributed transverse forces along X-brace
$g(x)$ = distributed compressive forces along X-brace
k = correction factor to moment equation, see Eq. (1)
l = length of brace, center to tip
l' = length of diagonal tension tape in canopy, center to tip
l_0 = length of column brace
m = mass, total mass of descending system
n = load factor
p = internal brace pressure
r = brace radius
t = material thickness
v_0 = freestream velocity
x, y, z = system of coordinates in canopy, see Fig. 7
α = arctg $(1/K)$, see Fig. 9
β = angle at tip of diagonal tension tape
γ = angle of diagonal tension tape at canopy center point
ρ = material density
σ = hoop stress in brace tube

Subscripts

a = atmospheric
b = braces
c = canopy
d = decelerator
p = payload
0 = braces plus payload
1 = refer to unit area

Presented as Paper 71-401 at the AAS/AIAA Variable Geometry and Expandable Structures Conference, Anaheim, Calif., April 21–23, 1971; submitted April 27, 1971; revision received December 10, 1971. This research has been supported by NASA Langley Research Center (Contract NAS1-9881). Previous contracts have been with NASA/LRC and NASA/GSFC.

Index categories: Sounding Rocket Systems; Optimal Structural Design.

* Senior Engineer.

Introduction

THE design and development of high-altitude parachutes for rocket-launched meteorological sonde systems is based on a set of requirements and constraints, which are somewhat unique among the wide variety of applications of aerodynamic decelerators. Typically, the sondes may be instrumented to measure and transmit atmospheric pressure and temperature, while altitude wind conditions are determined by tracking the descending system.

To let the sonde descend as slowly as possible, a minimum ballistic coefficient b is desired. To achieve this, the optimum combination of decelerator mass, payload mass, and drag area AC_D is required. In practice the design of the decelerator may be limited by considerations of packaging volume available, payload mass, and minimum dynamic pressure at which deployment is possible, before the structurally optimum design is achieved.

Parachutes presently in use for deployment at altitudes ranging from 45 to 80 km are self-inflated, self-supporting pressure drag devices with shapes varying from flat or hollow cups to ram-air operated balloons. Canopy materials used are low-porosity fabrics, or solid films, with surface densities of 10–20 g/m^2. Generally, these parachutes are too heavy to operate at low-ballistic coefficients of less than 0.1 kg/m^2 required for use at higher deployment altitudes of up to 100 km. A typical example of a cup-shaped parachute is the 15-ft Gentex parachute[1] for Arcas-type sounding rocket applications. Suitable for altitudes of deployment of 55 km–65 km and a typical payload of 2 kg, the ballistic coefficient of the descending system is approximately 0.3 kg/m^2. A more recent development of a balloon shaped decelerator is the 7-ft Starute[2] that is flown operationally on the Loki-Dart with a 0.35 kg meteorological payload and a ballistic coefficient of 0.15 kg/m^2. The new Super Loki-Dart meteorological system will contain an advanced 12-ft Starute with a payload of 0.45 kg and providing a system ballistic coefficient of approximately 0.08 kg/m^2. In

order to descend at subsonic velocity from an altitude of 80 km, a system ballistic coefficient of 0.073 kg/m^2, or less, is required. Advanced lightweight sondes presently under development will have masses as low as 0.1–0.2 kg. Exploitation of the full potential of these sondes at the highest possible altitudes up to 100 km will be maximized if they are carried by an extremely lightweight decelerator.

This paper describes some aspects of the current development of such an extremely lightweight decelerator, the Stokes-flow parachute.† The concept of this parachute and its implementation as a functional device presents some marked deviations from previous high-altitude decelerator technology. The design takes advantage of minimum gage filaments that are used to form finely textured open-mesh structures of high drag-producing efficiency. The parachute is suitable for carrying small payloads that may weigh only a small fraction of its mass at ballistic coefficients that are close to those of the self-supported mesh (from 0.07 down to 0.01 kg/m^2, or even lower, as still lighter materials become available).

The Stokes-Flow Parachute

The principle of operation of the Stokes-flow parachute[3,4] relies upon two distinctive aspects: 1) Its aerodynamic drag is primarily of viscous origin, based on the high drag-producing efficiency of small bodies operating at Reynolds numbers below unity. The decelerator, therefore, has a large flat canopy of open filamentary mesh with a low-surface density. 2) The canopy cannot inflate and support itself aerodynamically, as pressure drag devices do. These functions are, instead, provided by braces attached to the canopy as structural support members. Figure 1 shows the elements of a basic brace configuration of the Stokes-flow parachute. The open mesh canopy consists of a knitted composite of aluminized Mylar tapes with a width of 0.25 mm and nylon monofilaments with a diameter of 0.04 mm. A typical mesh is illustrated in Fig. 2. Its solidity is 0.19, and it has a surface density m_1 of 5 g/m^2. Aerodynamic theory[3,4] predicts that this mesh produces drag coefficients inversely variable with tape Reynolds number and above 30–40 km altitude, approaching those of solid plates. At 80 km altitude and a velocity of descent of 270 m/sec, the estimated C_D is 0.7.

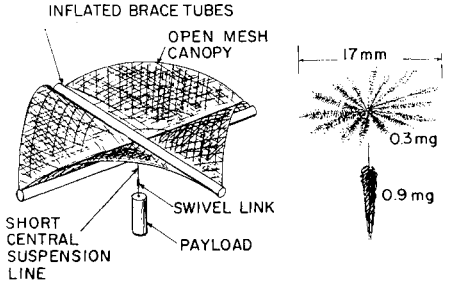

Fig. 1 Comparison of Stokes-flow X-brace parachute and dandelion seed.

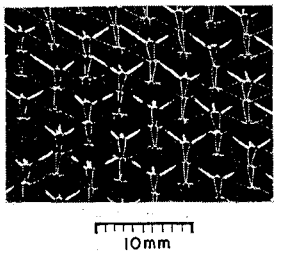

Fig. 2 Stokes-flow parachute knitted mesh.

† U.S. Patent No. 3,386,692.

The braces consist of two diagonally placed pressurized tubes of thin-film material, e.g., a 0.85 mil Mylar laminate with a Saran inner layer to reduce pinhole sensitivity. The lightweight payload is suspended from a single central suspension line.

The high-drag-producing efficiency of the Stokes-flow design is due to the low solidity of its canopy material, and to its low ratio of canopy surface area to projected area $A'/A = 1.15$. Additional anticipated features include: 1) virtual elimination of suspension lines to reduce tangling problems, 2) parachute is capable of deployment at very low-dynamic pressures, and 3) canopy stability even without a payload.

An added feature of the inflatable Stokes-flow parachute is its gradual collapse during descent. With an initial brace pressure of 98 torr the X-brace parachute is expected to collapse as it reaches 20–10 km altitude. Sea-level drop tests indicate that the drag coefficient of a fully collapsed X-brace parachute is of the order of 0.05, or 10–15 times lower than C_D of the fully deployed canopy. Velocity of descent is increased accordingly, at least three times, so that any undesirable dwelling time at lower altitudes, e.g., within controlled air space, is significantly reduced.

Nature has provided a strikingly similar example of a decelerator in the dandelion seed, with its tenuous structurally supported highly efficient canopy, as indicated in Fig. 1. Its surface density is of the order of 1.7 g/m^2, and its ballistic coefficient alone is approximately 0.00068 kg/m^2.

Several Stokes-flow parachute configurations under study use two or more X-brace canopies stacked behind each other, various forms of attachment of the canopy to the braces, and circular canopies with circumferential bracing. Braces may be inflatable tubes, foldable columns or coilable rods. Some aspects of these configurations will be discussed in subsequent sections.

Structural Analysis of X-Brace Parachutes

Analyses of Stokes-flow parachutes assume that design of the brace support is structurally critical; whereas, loading of the canopy is low enough that considerations of minimum gage, rather than maximum strength, are applied, at least with the presently available materials for canopy construction. Peak loading after deployment is expected to be of the order of 1.8 g's at 80–90 km altitude, and at an assumed initial velocity of 270 m/sec. However, loading at deployment becomes more severe and critical as altitude is decreased. At higher deployment altitudes loading due to maximum deceleration during descent becomes increasingly critical. Systems with low-ballistic coefficients are preferably deployed at higher altitudes.

Since a complete structural optimization of Stokes-flow parachute design would require an unwieldly number of parameters, procedures are aimed at emphasizing specific trade-offs, that establish guide lines for designs of minimum ballistic coefficients. Particularly useful trade-offs are those aimed at determination of: 1) optimum parachute size, 2) optimum configuration, and 3) optimum mesh. Items 1 and 2 are discussed in this paper. Results of optimum mesh studies are reported elsewhere.[5] Recommended mesh solidities are around 0.2 for operation at 70–100 km for the type of lightweight knitted mesh as illustrated in Fig. 2.

Optimum Size of Parachute

Consider a square X-brace parachute, as shown in Fig. 1, with inflatable tubular braces attached continuously along the canopy, and a single, central suspension line. The canopy is designed to billow up at a canopy rise angle of 25° between a sail center line and the plane of the braces. This angle is sufficient so that compressive forces due to canopy loading can be disregarded.[4,6] The braces are then loaded by transverse

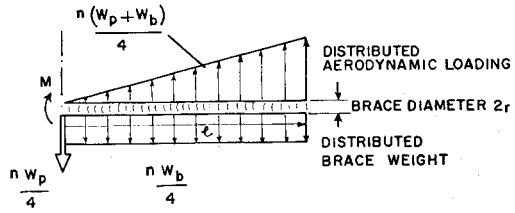

Fig. 3 Loading of X-brace with attached canopy.

continuous force distributions, as indicated in Fig. 3, which are counteracted by a moment of the inflated tube at the canopy center point. The canopy is assumed to support its own weight. An inflated thin-walled tube can carry a maximum moment M of

$$M = k\pi pr^3 = k\pi\sigma tr^2 = (n/24)l(4W_p + W_b) \quad (1)$$

The factor k takes values from 0.5 to 1, and is a function of the extent of the unwrinkled periphery of the loaded tube, and the level of its strain σ/E.[7] If the parachute is subjected to a deceleration of n g's, the required radius of the brace tube is

$$r = \frac{ngA\rho}{12k\sigma} + \frac{\left[\left(\frac{\pi}{3}ngAt\rho\right)^2 + 8\pi k\sigma tngm_p(A/18)^{1/2}\right]^{1/2}}{4\pi k\sigma t} \quad (2)$$

Total mass of the parachute (neglecting the single suspension line) is

$$m_d = m_b + m_c = \frac{2}{3g}B(2A^3)^{1/2}\left[1 + \left(1 + \frac{12g\,m_p}{B(2A^3)^{1/2}}\right)^{1/2}\right] + Aam_1 \quad (3)$$

where $B = \pi t\rho^2 g^2 n/2k\sigma$ is a structural brace parameter. Ballistic coefficient of the total system is

$$b = (m_b + m_c + m_p)/AC_D \quad (4)$$

The primary parameters of Eqs. (2–4) are those pertaining to material characteristics, parachute size, and payload. While m_c of a given mesh material increases with the square of size, Eq. (3) for m_b has cubic character. An illustration of Eq. (3) is given in Fig. 4 where m_d and m_b/m_c ratios are plotted for parachutes with various m_p, released at 100 km altitude and subjected to subsequent deceleration depending on b. The mesh of Fig. 2 is used for the canopy ($a = 1.15$), and braces are made of 0.85 mil Mylar laminate ($t = 2.16 \times 10^{-5}$ m, $\rho = 1.4 \times 10^3$ kg/m^3, $\sigma = 1.7 \times 10^7 N/m^2$, $E = 3.8 \times 10^9 N/m^2$, $k = 0.85$). Ballistic coefficients of these parachutes are shown in Fig. 5. The "square-cube law" produces shallow minimums on curves for b and m_b/m_c. As parachute size is further increased, these curves merge asymptotically toward the curve for $m_p = 0$. Note that the curves for $m_p = 0$ have their minimums at $A = 0$, representing conditions for the unsupported mesh without any bracing ($m_b = 0$). Parachutes shown in the curves weigh up to 8 times more than their assumed payloads, and the levels of b achieved indicate that subsonic velocities of descent at 80 km altitude are typical for this type of parachute. Figure 5 suggests that proper selection of decelerator size does not necessarily call for the largest size packable into the sounding rocket (see limits for Arcas rocket, typical for hand packaging at 0.32 g/cm^3. Note that this limit produces parachutes of various sizes, depending on m_p, because of varying brace radius requirements.) Selection is appropriately based on consideration of a trade-off between the acceptable limits of a penalty in descent performance vs economy, ease of handling, and reliability of deployment of a smaller parachute. A typical X-brace decelerator design for a 0.175 kg payload, presently under development, is summarized in Table 1. Characteristics of X-brace parachutes with substantially heavier payloads may require introduction of additional suspension lines, as reported elsewhere.[3,4]

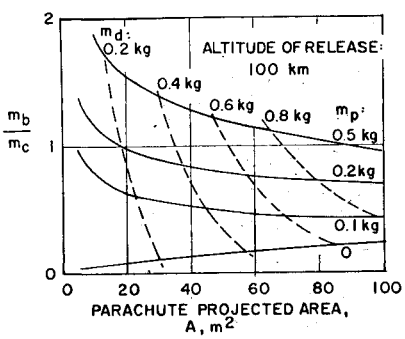

Fig. 4 X-brace parachute mass ratios.

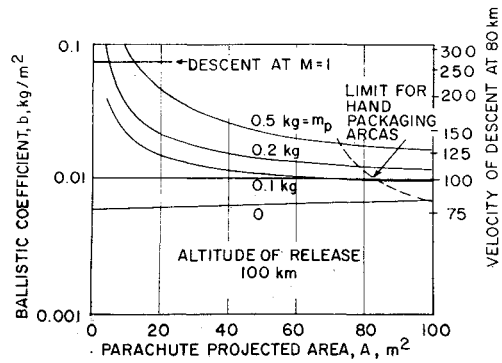

Fig. 5 Ballistic coefficient for X-brace parachutes.

Optimum Parachute Configuration

The preceding section considered parachute optimization with respect to size and assumed a predetermined configuration of design and composition of materials. Attention is now focused on variations of configuration while size is fixed. An appropriately defined canopy loading factor K is used as a variable in determining the payload carrying capability of a parachute. The optimum parachute carries the largest payload and has the lowest mass, if system's total mass is fixed. The configurations selected for study are X-brace parachutes with detached canopy and two different types of braces, to illustrate how strongly optimum design may vary for different support structures. As shown in Fig. 6a this parachute uses a square canopy which is attached to the diagonal braces by one center string and four strings at the corners. Design of the canopy is a flat square with a diagonal length of $2l'$. It is permitted to billow up in flight so that its projected diagonal

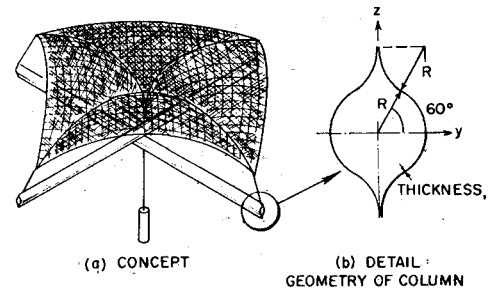

Fig. 6 Foldable column detached X-brace parachute.

Table 1 Comparison of Stokes-flow *X*-brace parachute designs[a]

Characteristic	Basic *X*-brace inflated tubes	Detached *X*-brace foldable columns	Detached *X*-brace inflated tubes
Canopy			
Characteristic parameter,	$\alpha = 25°$	$K = 1.800$	$K = 1.000$
A'/A;	1.15	1.490	1.170
Braces			
Characteristic dimension, m	r: 0.044	R: 0.016	r: 0.056
Thickness, t ($m \times 10^5$)	2.160	10.000	2.160
Total length, $4l_0$ (m)	10.600	10.800	10.800
Level of hoop stress, σ ($N/m^2 \times 10^{-7}$)	2.500	...	2.500
Internal pressure, p (torr)	98.000	...	73.000
Breakdown of Masses			
Canopy, m_c (kg)	0.081	0.105	0.082
Braces, m_b (kg)	0.089	0.230	0.142
Accessories (susp. line, swivel) m_a (kg)	0.020	0.030	0.030
Press. substance (isopentane) m_s (kg)	0.017	...	0.022
Decelerator, m_d (kg)	0.207	0.365	0.276
Total, m (kg)	0.382	0.540	0.451
m_b/m_c	1.100	2.190	1.730
m_d/m_p	1.180	2.080	1.580
Ballistic coefficient, b (kg/m^2)	0.039	0.055	0.046

[a] $A = 14\ m^2$, $m_p = 0.175$ kg, $n = 1.8$.

length is reduced to $2l$ of area, $A = 2l$. The payload is suspended from a single central suspension line. This concept is attractive because it allows packaging of braces and canopy into completely separate spaces. The following two types of braces are considered: 1) a foldable or rollable cylindrical column[8] with a quasibiconvex cross section, composed of two preformed sections of laminated Mylar sheet standing on edge, as shown in Fig. 6b, and 2) inflatable thin-walled tubes similar to those of the attached canopy *X*-brace parachute.

General loading conditions of a detached canopy *X*-brace parachute are shown in Fig. 7. The canopy is assumed to be composed of four sets of load-carrying single tapes parallel to the canopy edges. Adjacent sets are joined along diagonals by a load-carrying tape attached to the canopy suspension strings. Aerodynamic loading is distributed uniformly over A, and all local aerodynamic forces are vertical. The canopy supports its own weight. Under the influence of aerodynamic loading the shape of the canopy tapes is parabolic and all tapes have geometrically similar shapes. Diagonal tension tapes l' are loaded by continuously distributed transverse forces $f(x)$ and compressive forces, $g(x)$. Forces in the tension tapes T_0 and T_1 are functions of canopy force components F_0 and F_1 determined by force equilibrium equations, to yield

$$F_0/4 = nW_0/12 \tag{5}$$

$$F_1 = nW_0/6 \tag{6}$$

where n is the load factor and W_0 is the weight of payload plus braces. Since the amount of billowing, $l'/l = (a)^{1/2}$, is the same in the canopy edge tape and the diagonal tension tape, angles β and γ can be determined[6] if the shape of the diagonal tension tape is known

$$z^*/l = -X(x^*/l) + 0.333\,Y(x^*/l)^3 \tag{7}$$

with

$$X = (K - \operatorname{ctg}\gamma)/(K \operatorname{ctg}\gamma + 1)$$

$$Y = 3(1 + K^2)^2/(K^4 \operatorname{ctg}\gamma + K^3)$$

and where

$$K = nW_0/2lH_1 \tag{8}$$

is the canopy loading parameter. Axis x^* is inclined to x of Fig. 8 by an angle, $\alpha = \operatorname{arctg}(1/K)$.

With known loading conditions in the canopy, loading of the braces is determined and can now be used for the design of the foldable column braces. Neglecting the weight of the braces and assuming that F_1 is applied about the axis z of the smallest moment of inertia J of the cross section, then the moment of external loads on the column l_0 which is clamped in the center point, is

$$M = \frac{F_1 l_0}{1 - \dfrac{4l_0^2 F_1}{\pi^2 EJ \operatorname{tg}\beta}} = ER^2 t \tag{9}$$

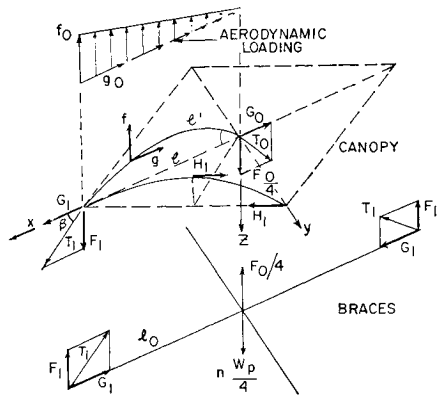

Fig. 7 Detached canopy *X*-brace parachute—loading of canopy and braces.

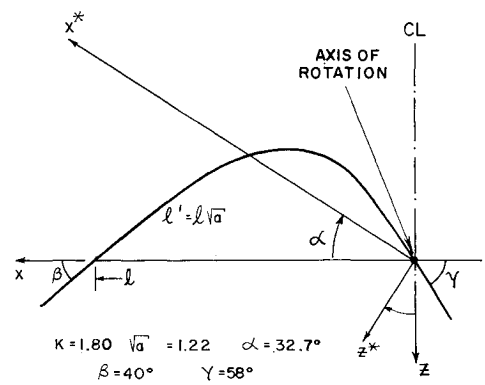

Fig. 8 Geometry of diagonal tension tape for optimized detached *X*-brace canopy.

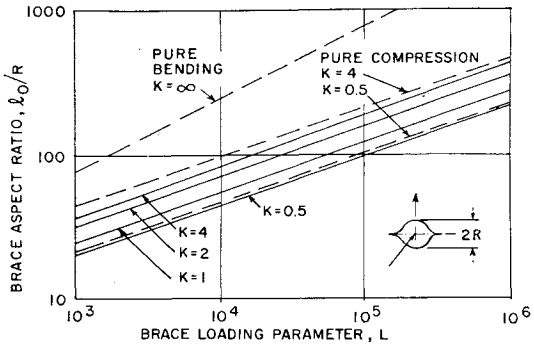

Fig. 9 Detached canopy X-brace parachute—column design data.

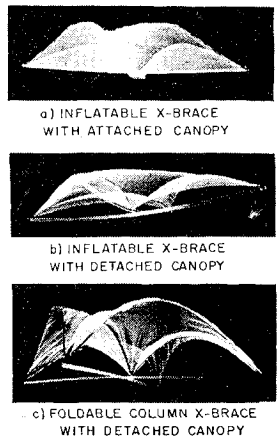

Fig. 11 Typical X-brace model parachutes ($A = 2.25$ m^2).

where

$$J = 3.41tR^3 \tag{10}$$

Introducing a brace loading parameter, L, defined as

$$L = Etl_0/nW_0 \tag{11}$$

Equation (9) with the help of Eqs. (6) and (10) is transformed as follows:

$$L = \frac{0.1667\left(\frac{R}{l_0}\right) + 0.0215 \operatorname{ctg}\beta}{\left(\frac{R}{l_0}\right)^3} \tag{12}$$

Brace aspect ratio l_0/R vs L is plotted in Fig. 9 for several canopy loading parameters, K. Total mass of parachute can now be determined as

$$m_d = m_c + m_b = m_1 aA + 38 l_0 Rt\rho \tag{13}$$

Figure 10 shows curves representing m_b/m_c and m_p vs K for several system total masses pertaining to parachutes of size $A = 14$ m^2, and subjected to a load factor of 1.8. The mesh shown in Fig. 2 is used for the canopy, and the brace columns are made of Mylar laminate of total thickness, $t = 10^{-4}$ m ($E = 3.8 \times 10^9$ N/m^2, $\rho = 1.4 \times 10^3$ kg/m^2). According to Fig. 10, optimum design is at a $K \sim 2$–2.2, slightly increasing as m increases. The dropoff of payload carrying capability toward low K is characterized by large ratios of m_b/m_c when a heavy brace is loaded predominantly in compression caused by a very flat canopy. According to Fig. 9, curves for pure compression and with $K \to 0$ show the lowest l_0/R ratios. On the other hand, m_p falls off as $K > 2.2$ because of excessive canopy mass, characterized by small m_b/m_c and approaching the pure bending curve of Fig. 9, where the brace aspect ratio is largest. Data for a parachute with $K = 1.8$ and $m_p = 0.175$ kg are given in Table 1. The shape of a diagonal tension tape

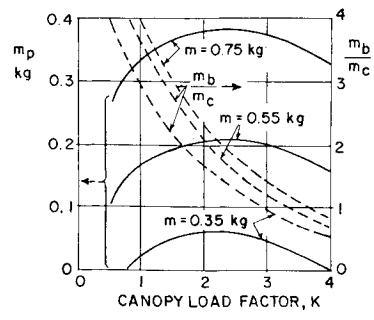

Fig. 10 Foldable column detached X-brace parachute—m_p and m_p/m_c for $A = 14$ m^2, $n = 1.8$.

of this design with considerable billowing, and according to Eq. (7), is shown in Fig. 8.

If an analysis similar to the foregoing is applied to detached canopy X-brace parachutes using inflatable tubes as braces, optimized parachute designs have typically flat canopies with a loading parameter K of about only 0.5. As Fig. 11 shows, this canopy is considerably flatter than those of the basic X-brace parachute and the optimized foldable column X-brace parachute. However, drop tests with subscale model showed that parachutes having a canopy with $K = 0.5$ were unstable and developed tilting and gliding. When the canopy load factor was increased to $K = 1$, the instability disappeared. Data for such a slightly off-optimum parachute for a payload of 0.175 kg and $n = 1.8$ are given in Table 1 for comparison with other X-brace designs.

Drop Tests with Model Parachutes

Drop tests with subscale model parachutes served to provide some verification of structural analyses under flight conditions. The models of scale 1:2.5 had a projected area, $A = 2.25$ m^2, and they were made of the same materials as their full-scale counterparts of $A = 14$ m^2 listed in Table 1. The experiments were performed under sea-level atmospheric conditions using a maximum available height of fall of approximately 27 m. Critical loading conditions of the brace were determined by varying mass of payload and/or internal brace pressure, where applicable. The critical point was recognized by visual observation during descent of partially or fully collapsed canopies. The photographs of Fig. 11 show three types of X-brace parachutes tested: a) the basic X-brace, $r = 10$ mm, $m_d = 49$ g; b) the detached canopy inflatable X-brace, $r = 15$ mm, $m_d = 47$ g; and c) the detached canopy foldable column X-brace,

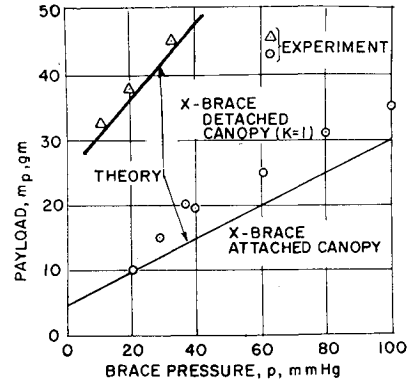

Fig. 12. Critical loading of inflatable X-brace model parachutes.

$R = 4.4$ mm, $m_d = 76$ g. Some results of the experimental drop tests with inflatable braces are shown in Fig. 12, demonstrating critical conditions for collapse. Actual collapse usually occurred in one of the two braces at the canopy center point. The theoretical estimates indicated are based on an equation for the moment of collapse of an inflated brace tube which includes some effects of residual stiffness in the tube walls,

$$M = \pi p r^3[1 + c(\pi E/p)(t/r)^2] \quad (14)$$

where $c = 0.2$ is an empirical constant.

The still favorable result of Fig. 12 may indicate that c should be larger, of the order of 0.4. The discrepancy can also be explained by a minor deviation from the assumed linear distribution of transverse loading due to aerodynamic forces. Because of the rapidly decreasing relative magnitude of the stiffness term as r is increased, this correction is not included in any full-scale calculations.

Drop tests with the foldable column braces indicated collapse of the canopy at a payload of 60 g, compared to a theoretical prediction of 86 g. The braces exhibited pronounced in-plane blowing just before collapse; whereas in the collapsed condition, they turned upward out of plane, with a twist located near the center point. Future investigation should include considerations of the column's torsional stiffness.

Packaging and Deployment

Experience gained during early experiments of packaging and deploying inflatable Stokes-flow decelerators[3] revealed three major critical areas contributing to unsuccessful deployments: 1) the susceptibility of brace tube materials to pin holes, causing leakage and early collapse of parachutes; 2) the susceptibility of an unfurling canopy to snarling with deploying braces and suspension lines, if any; and 3) the explosive and often destructive action of deployments in which evaporation of the pressurizing substance was uncontrolled. Progress is being made in all three areas as better film materials become available (e.g., Mylar laminate with Saran inner liner), as the number of suspension lines has been reduced to one single line, as ways are found to slow deployment action of pressurized tubes by controlled injection of the evaporating substance, and as noninflatable foldable column braces are investigated.

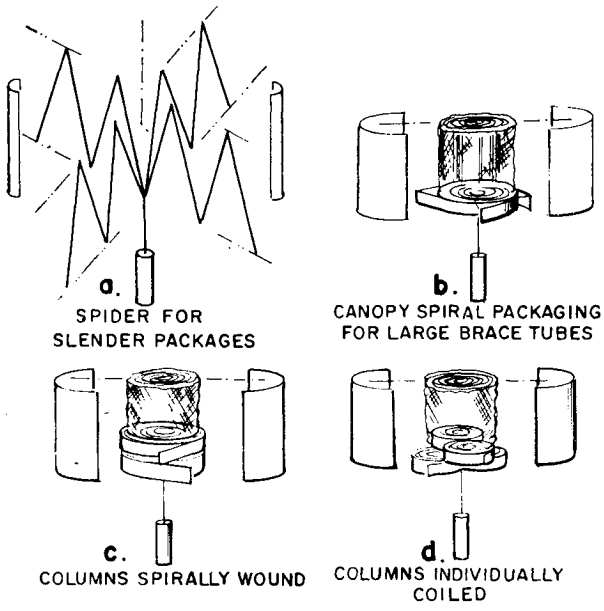

Fig. 13. X-brace parachute packaging patterns.

The sketches of Fig. 13 illustrate some of the more recent packaging patterns.

Presently, packaging density of Stokes-flow parachutes is limited to values of the order of 0.32 g/cm^2 (20 lb/ft^3), which is typical for hand packaging. Tighter packaging of braces is desirable to reduce residual air effects if it does not increase susceptibility to pin holes. Packaging of foldable column braces is limited by consideration of the smallest radius the flattened column can stand without suffering plastic deformation. This radius is of the order of tE/σ and is approximately 1 cm for the column brace Table 1. Packaging into deployment bags is undesirable because of frictional effects during rapid deployment. Wrapping into Teflon cloth, between staves, or packaging between foam-padded staves is more appropriate.

Controlled inflation of braces is achieved by separate storage of the pressurization liquid and by its injection at a pre-determined rate into the deploying brace. The liquid is stored in a separate pocket within the brace and is released through a very small orifice. The result is to slow down deployment from a fraction of a second to, typically, a period of 1–2 sec, to avoid catastrophic brace failure. The amounts of isopentane listed for the inflatable braces of Table 1 are based on an initial temperature of 250° K at which the parachute should remain deployed when subjected to a deceleration of $n = 1.8$. This drop of temperature from its value at sea level would be caused by evaporation and expansion of the pressurizing substance. Subsequent heating by exposure to solar radiation to a temperature of 300° K will increase internal brace pressure, and hoop stress at this stage is assumed to be the governing design criterion. The levels of σ in Table 1 are conservative to allow for overpressurization. The parachute will start gradually to collapse at approximately 20 km altitude.

Conclusion

This paper describes some characteristics of structural design of three types of X-brace parachutes of the same size and for the same payload. Although their configurations are markedly different, their descent characteristics should be similar.

The attached canopy inflatable X-brace parachute would provide the slowest descent and it can be hand packaged into the smallest volume (650 cm^3).

The detached canopy inflatable X-brace parachute has some undesirable aerodynamic characteristics in its optimized design with a very flat canopy. These deficiencies can be corrected with a moderate increase in canopy billowing. Its velocity of descent would be about 8% faster than the attached-canopy parachute, and its packaged volume is 871 cm^3.

The detached canopy column X-brace parachute would have the fastest descent of the designs analyzed; its velocity is faster by about 20%. Packaging volume is approximately 1000 cm^3 and it requires a diameter of 10 cm to accommodate the rolled brace columns at a packaging density of 0.42 g/cm^2 for joint wrapping of all brace legs. The major advantage of this design is its self-erectability on the basis of elastic forces rather than expanding gases. This parachute would not collapse during descent, and its low velocity toward sea level would be of the order of 1 m/sec.

All three designs are easily packaged into a sounding rocket of the Arcas type with a stowage capacity of 2100 cm^3. X-brace parachutes can operate under conditions where their mass may be substantially larger than the mass of the payload and the range of their lower ballistic coefficients would allow 30–60% lower velocities during subsonic descent of lightweight sondes from 80 to 90 km altitude. Some further improvement of this performance is possible by increasing canopy size. Additional improvements will be possible whenever new lightweight high-strength films and open canopy meshes are developed and become available.

References

[1] Bollermann, B., "A Study of 30 km to 200 km Meteorological Rocket Sounding Systems," *Literature and Data Review*, CR-1529, Vol. 1, Pts. 1 and 2, May 1970, NASA.

[2] Graham, J. J., "Ballute Development for Loki-Dart and Arcas Rocketsondes," AFCRL-68-0622, Nov. 1968, Air Force Cambridge Research Labs.

[3] Niederer, P. G., "Development of a High-Altitude Decelerator," CR-66755, Jan. 1969, NASA.

[4] Niederer, P. G., "Development of an Extremely Lightweight High-Altitude Decelerator," *Journal of Spacecraft and Rockets*, Vol. 6, No. 11, Nov. 11, 1969, pp. 1274–1278.

[5] Niederer, P. G. and Lewis, W. F., "Development of a High-Altitude Decelerator: Review and Evaluation of some Lightweight Knitted Canopy Meshes," Rept. ARC-R-362, Jan. 1970, Astro Research Corp., Santa Barbara, Calif.

[6] Niederer, P. G., Lewis, W. F. and Adams, L.R., "Development of a Stokes-Flow Decelerator for High-Altitude Meteorological Rocket Applications," Final Rept. on Contract NAS1-9881, Rept. ARC-R-513, Nov. 1971, Astro Research Corp., Santa Barbara, Calif.

[7] Topping, A. D., "Buckling Resistance of Inflated Cylinders in Bending," Rept. GER-13015, March 1967, Aerospace Corp., Santa Barbara, Calif.

[8] Crawford, R. F., "Strength and Efficiency of Deployable Booms for Space Applications," AIAA Paper 71-396, Anaheim, Calif, 1971.

MAY 1972 J. SPACECRAFT VOL. 9, NO. 5

Crippling and Buckling of Corrugated Ring-Stiffened Cylinders

DAVID BUSHNELL*
Lockheed Palo Alto Research Laboratory,
Palo Alto, Calif.

A finite-difference energy method is used for prediction of crippling, local buckling, and general instability. Reasonably good agreement is obtained between test and theory for shells which cripple due to pure axial compression, shells which cripple due to axial compression combined with hoop compression induced by local radial restraint at rings and boundaries, shells which buckle locally due to axial load path eccentricity, and shells which buckle between ring stiffeners. Crippling loads are calculated by treatment of a portion of the corrugation-sheet combination as a shell of revolution with radius very large compared to a typical dimension of the corrugation. Critical loads for buckling between rings are rather strongly dependent on boundary conditions load eccentricity, and length of cylinder, even for cylinders with many bays.

Introduction

THE purpose of this paper is to present the results of some analytical studies of axially compressed, semisandwich, corrugated cylinders representative of payload shrouds for various space systems applications. Ring-stiffened cylinders are analyzed for stress and stability through use of the BOSOR3 computer program.[1] Comparisons are made between test and theory and between various analyses. Effects of ring stiffeners, eccentric loading, boundary conditions, torsional stiffness, and combined mechanical and thermal loading are explored.

The analysis applies to semisandwich, corrugated flat panels and cylindrical shells reinforced by internal z-section rings. The corrugation geometry is given in Fig. 1a, and the ring stiffener geometry in Fig. 1b. In the BOSOR3 analysis, the corrugation is assumed to be bonded to the skin over the entire length d and the rings are treated as discrete structures. The aluminum shell and rings remain elastic.

Figures 2–5 show various types of buckling in corrugated panels and cylinders. Figure 2 shows part of a 12-in.-long and 9.75-in.-wide panel crippled by an axial load/length of

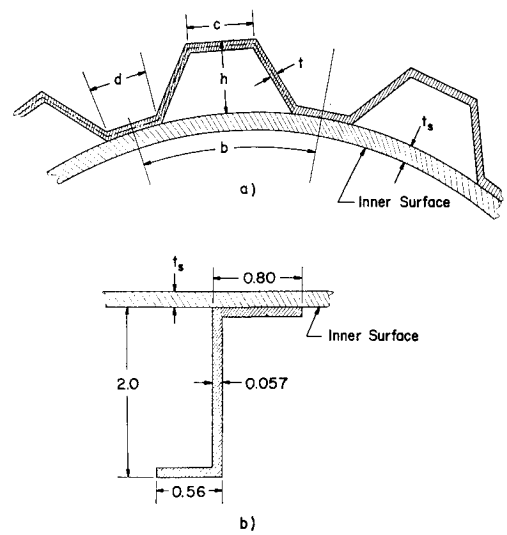

Fig. 1 a) Semisandwich corrugated wall geometry, and b) Internal discrete ring geometry.

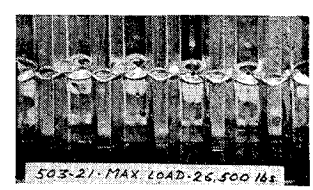

Fig. 2 Part of 9.75 in. × 12 in. panel with t = 0.020 in., t_s = 0.032 in. crippled under axial compression.

Received June 1, 1971; presented as Paper 72-138 at the AIAA 11th Aerospace Sciences Meeting, New York, January 17–19, 1972; revision received January 20, 1972. This work is sponsored by the Lockheed Independent Research and Independent Development Programs. The author is grateful for the many fruitful discussions with P. Stern, B. Burns, D. Tenerelli and B. Almroth during the course of this work.

* Staff Scientist. Associate Fellow AIAA.